ASTRO SCOUT: Autonomous Soft-growing Transformable RObotic System for Surface & Cavity Observation via Unfurling Toolset

Nelson G. Badillo Pérez
John A. Paulson School of Engineering and Applied Sciences
Harvard University
Cambridge, MA, USA
nbadilloperez@g.harvard.edu

Matthew L. Robinson
NASA Jet Propulsion Laboratory
California Institute of Technology
Pasadena, CA, USA
matthew.l.robinson@jpl.nasa.gov

Robert D. Howe
John A. Paulson School of Engineering and Applied Sciences
Harvard University
Cambridge, MA, USA
howe@seas.harvard.edu

***Abstract*—Lunar pits and lava tubes are high-priority exploration targets, yet no existing robotic platform can fully access their confined interiors for contact and proximity science. We present a mission concept for a pressure-driven soft growing robot capable of deploying from a lander at a lunar pit rim, descending to the pit floor, and exploring subsurface conduits. The system grows via tip-localized eversion, requiring no traction, grip points, or articulated joints, while its compliant body passively conforms to irregular terrain and enters highly confined openings. We present a composite membrane architecture using space-qualified materials and validate thermal feasibility across all mission phases through radiative-equilibrium analysis. The complete system mass of approximately 45 kg with a 260 m deployment reach enables integration as a secondary lander payload, addressing a capability gap in lunar subsurface exploration inaccessible to rigid platforms.**

Keywords— soft robotics, vine robot, lunar exploration, lava tube, space robotics, eversion

I. Introduction

As humans prepare for a sustained lunar presence, robotic technologies are becoming increasingly critical for exploring and mapping terrain. Lunar pits, over 200 identified from orbital data with diameters of 10-100 m and depths exceeding 100 m [1,2,3], are high-priority targets that contain preserved stratigraphic records of lunar evolution and represent potential sites for long-term settlement. These pits feature funnel-like openings with steep walls, overhangs, and regolith-covered floors [3]. Mare Tranquillitatis, a well-studied lunar mare pit, experiences temperatures ranging from 100°C to 135°C on its walls during the lunar day [4]. Radar has confirmed subsurface conduits beneath its overhangs [5] that may connect to extensive lava tube networks with benign 17°C isothermal conditions throughout the lunar day cycle [4], while also providing protection from non-ionizing and ionizing radiation [6] and abrasive regolith. These areas have been identified as among the best candidates for permanent human settlement [7].

Despite demonstrated surface operations [8,9], no existing platform can fully access these subsurface environments. We propose a soft growing robot platform based on vine robots [10], which extend new material at the tip through eversion driven by a positive pressure gradient generated by a working fluid, minimizing frictional environmental interactions. Their lightweight construction, high length-to-diameter ratio, compact packaging, and minimal control needs [11] make them ideal for navigating confined, largely unknown pit terrain. Vine robots have been demonstrated in terrestrial environments including archaeological sites [12] and search-and-rescue scenarios [13], but their implementation in extreme space environments and the corresponding design considerations have yet to be explored.

II. Mission Concept

The proposed system is a daughter-type robotic concept composed of a ground station, a deployable soft membrane, and tip-mounted instruments (Fig. 1.) The base station contains a compact material reservoir, a working fluid tank, and avionics that manage power and data transmission. During operation, the system is deployed by a lander from the edge of the pit; the lander relays communications and provides power.

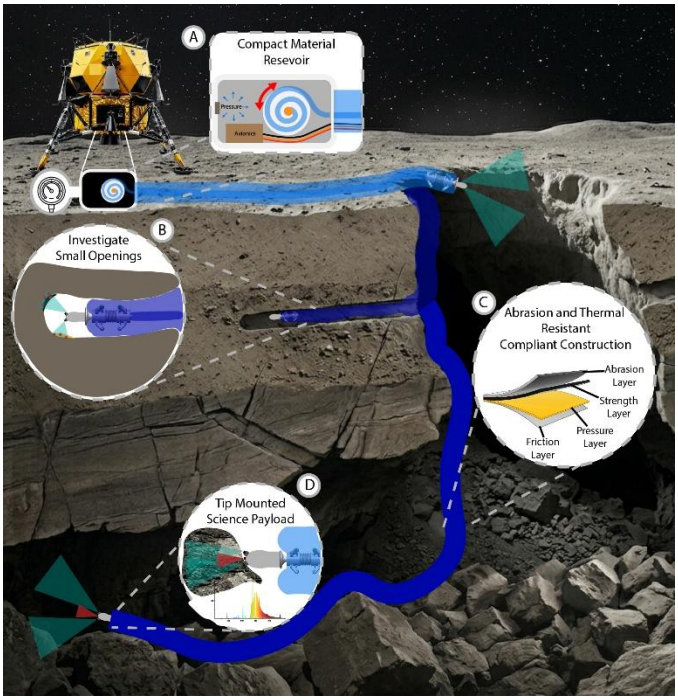

Figure 1. Soft growing robot mission concept. (A) material is extruded from the pressurized base via eversion. (B) the robot rappels down steep slopes and investigates small crevices. (C) the membrane is composed of flight heritage layers. (D) the robot performs scientific measurements deep inside the lunar pit.

Operation proceeds as follows. The base is pressurized above the membrane eversion threshold, and a motorized spool meters material under position control while pressure compensates for slack; tail tension provides indirect sensing of growth state and contact. As the body everts (Fig. 2), tip-mounted stereo imagers ride at the growing tip to map the descent, and the compliant body passively deforms into sub-diameter crevices that may lead to larger cavities. On the floor, the robot continues growing along the surface for spatial coverage. The membrane retracts via a tip-mounted retraction device [14]; if compromised, it can be severed at the base and re-extruded with fresh material.

The baseline relies on passive terrain navigation, appropriate for unmapped confined geometries where active steering is risky. Established steering mechanisms such as pneumatic muscles [13,15], tendon actuation [12], and pre-formed bends [16] could be retrofitted, but each adds mass and requires thermal-vacuum qualification. We defer them to future work.

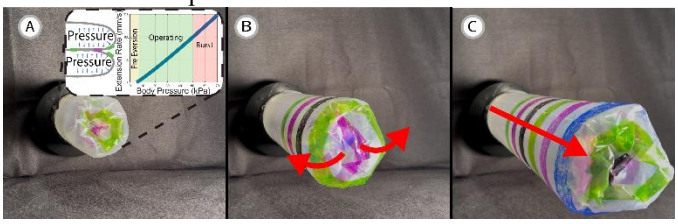

Figure 2. Vine robot eversion behavior. (A) membrane remains stowed below eversion pressure (yellow region) (B) central membrane material exits at the tip above this pressure (green region) and (C) extends the robot length.

Table 1 compares the proposed system against existing mission concepts: Daedalus, a tethered spherical robot with LiDAR for mapping [17]; Moon Diver, a dual-wheeled tethered rover for rappelling and delivering spectrometers, imagers, and contact science tools [18]; ReachBot, a multi-extendable limb robot for inverse manipulation [19] with its MELT concept of operations using a SuperCam array for contextual and spectroscopic analysis [20,21]; and cooperative heterogeneous robotic teams for combined surface and subsurface exploration [22]. The proposed system occupies a unique niche by leveraging its deformable body, eversion behavior, compact stowage, and low mechanical complexity to access terrain that rigid systems fundamentally cannot. This comes at the cost of limited: repositioning, manipulation capability, and payload capacity. Thus, suggesting the system is complementary to, rather than a replacement for, rover-based exploration.

Table 1. Comparison of proposed subsurface exploration concepts across capability metrics relevant to lunar pit and lava tube access.

Capabilities	Soft-Growing Robot	Moon Diver (Axel)	DAEDELUS	ReachBot
Confined Space Access	Deformable body enters sub-nominal openings	Limited to tether-accessible walls and robot sized apertures	Cannot enter openings smaller than sphere diameter	Boom may reach into crevices, body cannot enter
Terrain independence	No traction or grip required	Needs wheel traction on slopes and flat areas	Needs rollable floor surface and adequate actuator deployment	Needs convex grasp features on walls
Repositioning Capability	Limited; retract and re-grow with constrained path control	Full repositioning via tether winch and wheel motion	Free mobility on floor	Full 3D repositioning
Vertical descent capability	Grows downward under gravity and pressure	Rappels up to allowable tether length	Lowered on tether	Climbs using boom tension
Mechanical Complexity	1 motor + 1 pressure regulator for basic design	2-wheel motors + winch + instrument actuators	Internal mobility actuators + LiDAR rotation	8 booms + 8 grippers + steering
Stowage Volume ratio	Membrane on spool; body is the tether	Rover-type vehicle + separate tether	Rigid sphere + separate tether	Central body + 8 stowed booms
Payload Capacity	Lightweight tools and sensors	Multiple contact and proximity science tools	Small proximity science payloads	Proximity science suite SuperCam

Strong Capability | Limited Capability | Absent Capability

III. System Design

A. Membrane Architecture

Current vine robot materials (LDPE, nylon with TPU or silicone coatings) are unsuitable for extraplanetary environments [23]. Critical design requirements parallel those of EVA suit design: radiation resistance, thermal shielding, ASTM E595 outgassing compliance, and high abrasion resistance [24], while also meeting vine-robot-specific needs for low eversion pressure, compact stowage volume, and lightweight construction. Table 2 compares traditional vine robot materials with space-qualified candidates across key performance metrics; no single material satisfies all requirements simultaneously, motivating a composite architecture.

Table 2. Potential material comparison. Material properties sourced from manufacturer datasheets [25-27], NASA technical publications [28-31], and published polymer permeability [32] and radiation studies [33].

Capabilities	LDPE	TPU-coated Ripstop Nylon	Kapton HN	Kapton FN (FEP-Coated)	Vectran HS	FEP Fluoropolymer
Thermal range	-50°C to 80°C	-40°C to 100°C	-269°C to 400°C	-269°C to 400°C	Cryogenic to +230°C; retains flex at Mars temps	-269°C to 205°C
Radiation Tolerance	Degrades at ~10kGy-50kGy	TPU degrades at ~10kGy	Stable up to 50MGy	Stable up to 50MGy	Stable up to ~5MGy; UV-Sensitive	Stable up to 5KGy
Gas barrier performance	Moderate; adequate for short-duration Earth operations	Moderate; for Earth-pressure differentials	Low permeability; improvement with aluminum coating	Low permeability; FEP adds secondary seal	High permeability; Porous woven structure	Low permeability
Abrasion resistance	Very poor; low cyclic life	Good; fabric weave resists tears	Poor; documented cyclic wear vulnerability	Poor; FEP improvement but insufficient	Excellent; proven against lunar simulant	Moderate as film; insufficient alone
Eversion compatibility	Excellent; standard literature material	Excellent; standard literature material	Unknown; testing required	Unknown; testing required	Unknown; testing required	Lowest friction; balloons without structural layer
Space heritage	None	None for space vacuum	TRL 9; all major missions	TRL 9; all major missions	TRL 9; Pathfinder, MER, MSL	TRL 9; Apollo EVA suits, Hubble

Strong Capability | Limited Capability | Poor Capability

The proposed four-layer composite comprises an outer PTFE-coated Vectran layer for abrasion resistance and a high reflectivity-to-absorption ratio; a woven Vectran structural restraint; an aluminized Kapton FN gas barrier, and an FEP inner liner for low gas permeability and low friction during eversion (Fig. 1(C)). This architecture is based on proven flight heritage [34-36]. Prototype fabrication and eversion testing of the composite laminate are ongoing, with particular attention to bending stiffness and the impact of lamination on eversion pressure. Eversion pressure scales with deployed length and path tortuosity due to tail-on-body friction; the closed-form quasi-static model of [11] is used in Appendix A to bound deployment reach and admissible cumulative turn angle.

B. Working Fluid

The working fluid must remain phase-stable across the thermal envelope, store densely during transport, and be inert with all membrane materials. CO_2's sublimation point (–78 °C) lies within the skylight-rim envelope at lunar night; helium permeates polymer films at orders-of-magnitude-higher rates than diatomic gases [37]; water solidifies at the cold end and adds mass. Nitrogen (N_2) is selected: gaseous above –196 °C, inert, with extensive flight heritage including recent lunar sampling [38].

The system uses open-loop pressure control: stored N_2 is expended during eversion and retained in the deployed membrane to maintain shape. Retraction follows the inversion mechanism of [14], with tube-volume reduction passively repressurizing the gas; a check valve enables partial recovery to a secondary reservoir without active pumping [39].

C. Tip Instrumentation

The tip payload performs proximity and contact science at locations inaccessible to wheeled platforms. A stereo camera pair provides 3D imaging of pit wall stratigraphy during descent and tube morphology during horizontal exploration [10,12]. A VNIR contact reflectance spectrometer (350-1000 nm range, under 200 g mass) with integrated LED illumination enables in-situ mineralogical identification of exposed basalt layers. An environmental sensor suite (temperature, radiation, pressure) measures habitability parameters along the full deployment path from surface to tube interior. Together, these instruments address priority science questions such as volcanic stratigraphy, mineralogical composition of subsurface rock, and the thermal and radiation environment relevant to future human habitation [7,18], in addition to performing critical spatial mapping tasks within these unknown confined spaces.

Tip payloads are mounted on a rigid cap that rides ahead of the eversion front, with internal cabling routed through a body-length pocket or within the pressurized membrane. This architecture is mechanically decoupled from the everting membrane and enables sensor swaps between deployments. Active tooling that must penetrate or sever the membrane (e.g., sample-acquisition end-effectors) remains an open design problem and is excluded from the present baseline.

IV. Feasibility Analysis

A. Thermal Feasibility

The deployed membrane must withstand the lunar thermal environment across three operational phases: sunlit surface traversal, skylight transition, and lava tube operation. The absence of a lunar atmosphere eliminates convective heat transfer, reducing the problem to radiative exchange between the membrane, the Sun, the surrounding terrain, and deep space [40]. The membrane's thin composite cross-section has negligible thermal conduction along its length, permitting a lumped-radiative-equilibrium model [41]:

$$\alpha S \cos(\theta) + \varepsilon_{mem}\varepsilon_{regolith}\sigma T_{regolith}^4 = 2\varepsilon_{mem}\sigma T_{mem}^4 \quad (1)$$

where α is the solar absorptance, $S = 1361\ W/m^2$ is the solar constant, θ is the solar incidence angle, ε values are thermal emittances of the membrane outer layer and regolith, and σ is the Stefan-Boltzmann constant. Using PTFE outer layer properties ($\alpha = 0.20$, $\varepsilon_{mem} = 0.85$) [42] with worst-case normal solar incidence on regolith at 111°C [4] and $\varepsilon_{regolith} = 0.95$, the equilibrium membrane temperature is 66°C; well within all composite material limits. In the skylight transition zone, the maximum temperature does not exceed this value. In the lava tube, the membrane equilibrium temperature converges to the isothermal wall temperature (17°C).

B. Mass Budget

For a 260 m deployment path (30 m surface traverse, 130 m descent, 100 m exploration margin) at a 127 mm diameter, membrane surface area is approximately 104 m^2. Using an estimated composite areal density of 300 g/m^2 (based on individual layer densities [25-27, 34]), membrane mass is 31 kg. At an estimated eversion pressure of 40 kPa and 20°C internal temperature, the ideal gas law gives a consumable N_2 mass of 1.5 kg. The calculated gas tank volume given a 34 MPa internal pressure and 54.2 mol of N_2 at a shielded internal temperature is 3.8L. Given similarities in avionics and pressure control architecture with flight-proven LISTER hardware [38], we adopt their 13 kg avionics mass estimate. Total system mass is approximately 45.5 kg. This is significantly below Moon Diver's 122.8 kg rover mass [18] and viable as a lander payload. The membrane accounts for 68% of total mass; optimization is possible through smaller diameters (e.g., 50 mm reduces membrane mass to 12 kg) or shorter traverse lengths. Per ANSI/AIAA S-120A-2015 [43], a 30% mass growth allowance is applied at this concept-development maturity (TRL 3-4 components), bringing the total margined system mass to 59 kg.

C. Power Budget

Peak power is dominated by the spool motor during eversion (30 W) and tip illumination LEDs (5 W); avionics, communications relay, and sensor sampling contribute 15 W average. Total estimated peak draw is 60 W with 30 W average, well within typical CLPS-class lander payload allocations. Detailed line items appear in Appendix B. Power scaling with deployed length is dominated by spool-motor torque, which grows with length.

V. Conclusion

This paper presented a soft growing robot mission concept for proximity and contact science in lunar pits and lava tubes. Comparison with existing concepts identified the niche vine-robot morphology fills: terrain-independent access to confined subsurface geometries without articulated mechanisms. A materials trade study motivated a four-layer space-qualified composite, and radiative-equilibrium analysis confirmed thermal feasibility across all phases. The 45 kg, 260 m system is viable as a secondary lander payload. Critical open risks are the unvalidated eversion behavior of the laminate and gas-barrier integrity under repeated folding in thermal-vacuum conditions. A natural mission architecture pairs the platform with a surface rover (e.g., Endurance-class [9] or a CLPS-scale platform) for context imaging and lander-relay redundancy; a science traceability matrix appears in Appendix C.

This is a concept paper; the principal limitation is the unvalidated 40 kPa eversion pressure for the proposed laminate, though it lies within bounds reported for comparable vine membranes. Material properties are largely literature-sourced; ongoing work validates them via mechanical and thermal-vacuum testing, including abrasion against JSC-1A simulant.

Anticipated failure modes are: puncture or abrasion from sharp regolith mitigated by the PTFE-coated Vectran outer layer and base-severance recovery; gas-barrier delamination under thermal cycling under evaluation in laminate-coupon testing; kinking or stall in tortuous paths exceeding the friction-limited turn budget (Appendix A) detected via tail tension and mitigated by retraction; eversion jamming at sub-diameter pinch points; and regolith electrostatic adhesion.

Future work targets composite manufacturing, field testing in terrestrial lava tubes, tool-set qualification for space deployment, and lander-mockup integration. The architecture extends naturally to multi-tool exchange and to growing tactile sensing for proprioception and contact characterization.

VI. References

[1] J. Haruyama et al., "Possible lunar lava tube skylight observed by SELENE cameras," Geophys. Res. Lett., vol. 36, no. 21, 2009.

[2] M. S. Robinson et al., "Confirmation of sublunarean voids and thin layering in mare deposits," Planet. Space Sci., vol. 69, no. 1, pp. 18-27, 2012.

[3] R. V. Wagner and M. S. Robinson, "Distribution, formation mechanisms, and significance of lunar pits," Icarus, vol. 237, pp. 52-60, 2014.

[4] T. Horvath, P. O. Hayne, and D. A. Paige, "Thermal and illumination environments of lunar pits and caves," Geophys. Res. Lett., vol. 49, no. 14, p. e2022GL099710, 2022.

[5] L. Carrer et al., "Radar evidence of an accessible cave conduit on the Moon below the Mare Tranquillitatis pit," Nat. Astron., vol. 8, no. 9, pp. 1119-1126, 2024.

[6] G. De Angelis et al., "Lunar lava tube radiation safety analysis," J. Radiat. Res., vol. 43, suppl., pp. S41-S45, 2002.

[7] R. P. Martin and H. Benaroya, "Pressurized lunar lava tubes for habitation," Acta Astronaut., vol. 204, pp. 157-174, 2023.

[8] J. M. Long-Fox, H. Campins, and D. T. Britt, "A review of technologies for lunar science, exploration, resources, and settlement," Planet. Space Sci., p. 106229, 2025.

[9] J. D. Baker et al., "The Endurance lunar rover sample return mission," in Proc. IEEE Aerosp. Conf., Mar. 2024, pp. 1-13.

[10] E. W. Hawkes et al., "A soft robot that navigates its environment through growth," Sci. Robot., vol. 2, no. 8, p. eaan3028, Jul. 2017.

[11] L. H. Blumenschein et al., "Design, modeling, control, and application of everting vine robots," Front. Robot. AI, vol. 7, p. 548266, Nov. 2020.

[12] M. M. Coad et al., "Vine robots: Design, teleoperation, and deployment for navigation and exploration," IEEE Robot. Autom. Lett., vol. 5, no. 2, pp. 853-860, Apr. 2020.

[13] P. A. der Maur et al., "Roboa: Construction and evaluation of a steerable vine robot for search and rescue applications," in Proc. IEEE Int. Conf. Soft Robot., Apr. 2021, pp. 15-20.

[14] M. M. Coad et al., "Retraction of soft growing robots without buckling," IEEE Robot. and Autom. Lett., vol. 5, no. 2, pp. 2115-2122, 2020.

[15] A. Kübler et al., "A multi-segment, soft growing robot with selective steering," arXiv:2212.03951, 2022.

[16] N. Agharese and A. M. Okamura, "Configuration and fabrication of preformed vine robots," arXiv:2306.01166, 2023.

[17] A. P. Rossi et al., "DAEDALUS—Descent and Exploration in Deep Autonomy of Lava Underground Structures," ESA OSIP Study, 2021.

[18] I. A. D. Nesnas et al., "Moon Diver: Exploring a pit's exposed strata to understand lunar volcanism," Acta Astronaut., vol. 211, pp. 163-176, Oct. 2023.

[19] T. G. Chen et al., "Locomotion as manipulation with ReachBot," Sci. Robot., vol. 9, no. 89, p. eadi9762, 2024.

[20] R. C. Wiens et al., "The SuperCam instrument suite on the NASA Mars 2020 rover," Space Sci. Rev., vol. 217, pp. 1-87, 2021.

[21] J. Di et al., "Martian Exploration of Lava Tubes (MELT) with ReachBot," in Proc. Int. Conf. Space Robot., Jun. 2024, pp. 36-41.

[22] R. Domínguez et al., "Cooperative robotic exploration of a planetary skylight surface and lava cave," Sci. Robot., vol. 10, no. 105, p. eadj9699, 2025.

[23] Y. Zhang et al., "Progress, challenges, and prospects of soft robotics for space applications," Adv. Intell. Syst., vol. 5, no. 3, p. 2200071, 2023.

[24] P. Weiss et al., "Advanced materials for future lunar extravehicular activity space suit," Adv. Mater. Technol., vol. 5, no. 9, p. 2000028, 2020.

[25] DuPont, "Kapton polyimide film general specifications," datasheet EI-10167, 2019.

[26] DuPont, "Kapton FN polyimide film," datasheet EI-10160, 2006.

[27] Kuraray Co., Ltd., "Vectran-Liquid crystal polymer fiber," aerospace datasheet, 2020.

[28] R. B. Fette and M. F. Sovinski, "Vectran fiber time-dependent behavior and additional static loading properties," NASA TM-2004-212773, 2004.

[29] J. R. Gaier and E. A. Sechkar, "Abrasion of candidate spacesuit fabrics by simulated lunar dust," NASA TM-2009-215800, 2009.

[30] NASA, "Wire insulation selection guidelines," NEPP Program.

[31] P. McGarey et al., "Design and test of an electromechanical rover tether for the exploration of vertical lunar pits," in Proc. IEEE Aerosp. Conf., Mar. 2020, pp. 1-10.

[32] H. Jung et al., "Investigation of gas permeation through Al-metalized film for vacuum insulation panels," Int. J. Heat Mass Transf., vol. 56, pp. 436-446, 2013.

[33] A. Cryer et al., "Radiation impact on robot-relevant polymers for high gamma environments," Radiat. Phys. Chem., vol. 235, p. 112745, 2025.

[34] ILC Dover, "Development and evaluation of the Mars Pathfinder inflatable airbag landing system," Acta Astronaut., vol. 53, pp. 341-355, 2003.

[35] M. M. Finckenor, "Comparison of high-performance fiber materials properties in simulated and actual space environments," NASA MSFC, 2017.

[36] T. Jones and W. R. Doggett, "Time-dependent behavior of high-strength Kevlar and Vectran webbing," in Proc. AIAA SciTech Forum, 2014, paper AIAA 2014-1328.

[37] B. Flaconnèche, J. Martin, and M. H. Klopffer, "Permeability, diffusion and solubility of gases in polyethylene, polyamide 11 and poly (vinylidene fluoride)," Oil Gas Sci. Technol., vol. 56, no. 3, pp. 261-278, 2001.

[38] S. Nagihara et al., "The Lunar Instrumentation for Subsurface Thermal Exploration with Rapidity (LISTER)," Planet. Sci. J., vol. 6, no. 10, p. 232, 2025.

[39] J. L. Hall et al., "Prototype development of a variable altitude Venus aerobot," in Proc. AIAA Aviation Forum, 2021, paper AIAA 2021-2696.

[40] D. G. Gilmore, Ed., Spacecraft Thermal Control Handbook, Vol. 1, 2nd ed. The Aerospace Press, 2002.

[41] F. P. Incropera et al., Fundamentals of Heat and Mass Transfer, 7th ed. Wiley, 2011.

[42] J. H. Henninger, "Solar absorptance and thermal emittance of some common spacecraft thermal-control coatings," NASA Ref. Publ. 1121, 1984.

[43] ANSI/AIAA S-120A-2015, Mass Properties Control for Space Systems, American Institute of Aeronautics and Astronautics, 2015.

Appendix A: Pressure-Loss and Geometric Bounds

The quasi-static eversion model of Blumenschein et al. [11] decomposes driving pressure into a static yield term, viscoplastic loss from material everting, exponential friction from tail material moving through curves, and linear friction along straight sections. For our 260 m, 127 mm-diameter system at the baseline 40 kPa eversion pressure, the linear-friction term dominates straight-path operation, while the exponential term proportional to $e^{(\mu\theta)}$, where θ is the cumulative turn angle and μ is the tail-on-body friction coefficient sets the geometric envelope. Minimum bend radius is set by membrane bending stiffness rather than friction; lamination testing (ongoing) will refine this bound. Pinch points narrower than 50% of nominal diameter cause local pressure spikes that risk membrane damage; the severance capability (Section II) provides a potential recovery. These bounds are concept-level and will be refined experimentally.

Appendix B: Power Budget

Estimates assume continuous-eversion operation during deployment phase, with intermittent spectroscopy and continuous environmental sampling. Spool-motor power scales linearly with length and is the dominant load during eversion/inversion; communications and avionics estimates follow LISTER-class instrumentation [38].

Subsystem	Peak (W)	Avg (W)	Duty Cycle
Spool motor (eversion/inversion)	30	15	Active during growth
Pressure regulator	3	1	Active
Tip stereo cameras	4	4	Continuous
LED illumination	5	3	Subsurface only
VNIR spectrometer	6	0.5	Spot measurements
Environmental sensors	1	1	Continuous
Avionics+ comms	12	8	Continuous
Total	**~61**	**~32.5**	—

APPENDIX C: SCIENCE TRACEABILITY MATRIX

The matrix below maps each instrument to a specific lunar science priority, drawn from the decadal-survey objectives cited via [7] and [18].

Science Question	Measurement	Instrument	Phase
Volcanic stratigraphy of mare	High-res stereo imagery of pit walls	Stereo cameras	Descent
Mineralogy of subsurface basalt	VNIR reflectance, 350-1000 nm	Contact spectrometer	Floor + tube
Habitability for human settlement	Temperature, radiation dose, pressure	Environmental sensor suite	Full path
Subsurface void mapping	3D point cloud generation	Stereo cameras + LED	Tube interior